Optics Letters

Toward real-time volumetric tomography for combustion diagnostics via dimension reduction

Tao Yu, Hecong Liu, Jiaqi Zhang, Weiwei Cai,* and Fei Qi

Key Laboratory of Education Ministry for Power Machinery and Engineering, School of Mechanical Engineering, Shanghai Jiao Tong University, 800 Dongchuan Road, Shanghai 200240, China
**Corresponding author: cweiwei@sjtu.edu.cn*

Received 17 November 2017; revised 12 January 2018; accepted 29 January 2018; posted 31 January 2018 (Doc. ID 313404); published 27 February 2018

Volumetric tomography for combustion diagnostics is experiencing significant progress during the past few years due to its capability of imaging evolving turbulent flows. Such capability facilitates the understanding of the mechanisms behind complicated combustion phenomena such as lean blowout, acoustic oscillations, and formation of soot particles. However, these techniques are not flawless and suffer from high computational cost which prevents them from applications where real-time reconstructions and online monitoring are necessary. In this Letter, we propose a new reconstruction method that can effectively reduce the dimension of the inversion problem, which can then be solved with a minimum computational effort. This method and a classical iterative method were tested against each other using a proof-of-concept experiment in which endoscopic computed tomography of chemiluminescence (CTC) was implemented. The results show that the proposed method can dramatically reduce the computational time and, at the same time, maintain similar reconstruction accuracy, as opposed to the classical approach. Although this Letter was discussed under the context of CTC, it can be applied universally to other modalities of volumetric tomography such as volumetric laser-induced fluorescence.

OCIS codes: (280.1740) Combustion diagnostics; (110.6955) Tomographic imaging; (110.6880) Three-dimensional image acquisition.

https://doi.org/10.1364/OL.43.001107

The kilohertz-rate volumetric tomography has attracted increased research efforts for the past few years due to the recent progress in both high-speed cameras and high-power high-repetition-rate pulsed lasers [1–3]. For example, volumetric laser-induced incandescence was used to reconstruct the distribution of soot volume fraction of a turbulent diffusion jet flame [4]; volumetric laser-induced fluorescence has been utilized to image important intermediate flame species such as OH, CH_2O, and PAH in turbulent flames [2,3]; and volumetric computed tomography of chemiluminescence (CTC) was employed to track the ignition process of supersonic reactive flows [1]. The development of these methods provides an unprecedented opportunity to understand the complicated turbulent combustion phenomena such as the acoustic oscillations, soot formation, and lean blowout. However, these methods suffer from a few limitations that prevent their extended applications to practical scenarios. For example, there is typically limited optical access for engine measurements, and only a small number of projections are available for tomographic reconstruction. In addition, the experimental cost is usually unaffordable as a considerable number of expensive high-speed cameras are required. Both limitations can potentially be overcome by using inexpensive fiber bundles which are flexible and easy for deployment. Furthermore, a tomographic inversion typically involves the solution of a large linear equation system which has millions of variables [5]. The algebraic reconstruction technique (ART) and its variants are the most prevailing algorithms that have been adopted in the previous demonstrations [5–10]. They are typically inefficient due to their iterative nature [1,7,11,12]. The situation worsens for a tomographic system that operates at a kilohertz rate since thousands of frames needs to be processed within a second. Thus, the computational cost associated is formidable, and the reconstructions are usually performed offline [1–4,6,13–15]. This has become a major bottleneck that greatly limits volumetric tomography to applications where online monitoring of the combustion process is required. Thus, this Letter aims to propose an efficient inversion algorithm that can effectively downsize the large-scale linear equation system into a small one. Proper orthogonal decomposition (POD) is adopted here for this purpose [16]. This method expresses the reconstruction as a weighted summation of a few Karhumen–Loeve (KL) basis functions, formulating the inversion process as the determination of weight coefficients for these basis functions [17]. Since the number of basis functions is significantly smaller than the number of voxels i.e., the unknowns, the dimension of the inversion problem, as well as the computational cost, can be dramatically reduced.

The remainder of this Letter is organized as follows: the mathematical formulation of the endoscopic CTC and the mathematical background of POD are briefly described first;

the setup for a proof-of-concept experiment is then introduced, after which the reconstructions from both the proposed method and the ART algorithm are analyzed and compared; and a summary is provided to conclude this Letter.

As mentioned, a variety of tomographic techniques have been demonstrated previously for combustion diagnostics, and the principles behind them are similar. In this Letter, we cite the endoscopic CTC as an example to demonstrate the proposed method since an expensive excitation laser is not required. A typical endoscopic CTC system is illustrated in Fig. 1. As can be seen, three coordinate systems are defined, the origins of which are set on the reconstruction volume, the object lens in front of the receiving end of a fiber bundle, and the sensor chip on the camera, respectively. The geometric relationship between the coordinate systems can be determined through a calibration process, and the projection of any point within the reconstruction volume to the camera can then be predicted according to the coordinate transformation and the thin lens formula [5,18]. By discretizing the tomographic field into a number of I cubic voxels, a projection of the luminescent field is essentially the summation of images of the voxels formed on the camera sensor array, and the signal of the sth pixel on the tth projection can be mathematically expressed as

$$p_{s,t} = \sum_{i=1}^{I} f_i \cdot w_i(s,t), \tag{1}$$

where i and I are the voxel index and the total number of voxels, respectively; f_i is the luminescent intensity of the ith voxel; and $w_i(s,t)$ is the spread function of the ith voxel with the parameters s and t indicating the sth pixel of the tth projection, and can be calculated by tracing the projections of a large set of random points that are uniformly distributed within the voxel. Repeating Eq. (1) for every pixel of all projections, a linear equation system can be formulated as

$$\vec{p} = W \cdot \vec{f}, \tag{2}$$

where W is the weight matrix, and is the assembly of the spread functions of all voxels at each projection; $\vec{p}$ and $\vec{f}$ are the signal intensity of all pixels and the chemiluminescent intensity of all voxels arranged as column vectors, respectively. In practical applications, the field to be reconstructed is usually discretized into millions of voxels, leading to a large-scale linear equation system, the solution of which involves formidable computational cost. As mentioned earlier, the ART algorithm and its variants are iterative in nature, and it took around 30 min to solve the inversion problem as reported in [19]. Furthermore, in the previous demonstrations, the measured data were processed frame by frame without considering the common features among them. However, due to the continuity of the flame in the temporal domain, the connections between the consecutive frames should be taken full advantage of and serve as a most informative prior for tomographic reconstructions.

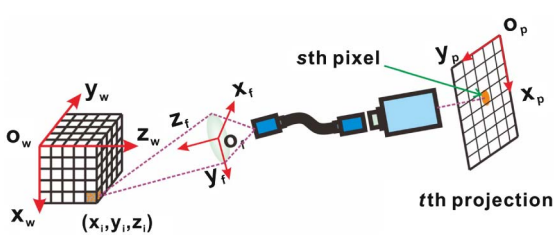

Fig. 1. Illustration of three coordinate systems defined for the mathematical formulation of endoscopic CTC.

In this Letter, we propose a new reconstruction algorithm to reduce the dimension of the problem so as to minimize the computational cost by extracting the dominant features of two training sets, one for the reconstructions and the other one for the corresponding projections. This is achieved by performing the POD [20] procedures twice (referred to as TPOD hereafter), each time on one of the training sets. The POD method is well-established and has been widely adopted in flow analysis [21,22]. Mathematically, it is equivalent to singular value decomposition [21] and can be described as

$$F = U\Sigma V^T = QV^T, \tag{3}$$

where F is a matrix with each of its column representing a sample in the training set of either the reconstructions or the projections; Σ is a diagonal matrix, and its diagonal elements are the singular values that are arranged in a descending order; and U and V are orthonormal matrices, respectively. The column vectors of V are essentially the basis functions for the training set.

Any field that needs to be reconstructed can then be approximated as a linear combination of a series of basis functions as

$$\vec{f} \approx \sum_{k=1}^{K} \alpha_k \vec{\psi}_k, \tag{4}$$

where $\vec{\psi}_k$ is the kth basis function of the reconstruction training set, α_k is the corresponding weighted coefficient, and K is the total number of the basis functions used for the approximation. Similarly, the measured projections can be represented as a weighted summation of a few dominant features as

$$\vec{p} \approx \sum_{q=1}^{Q} \beta_q \vec{\varphi}_q, \tag{5}$$

where $\vec{\varphi}_q$ is the qth basis function of the projection training set; β_q is the corresponding weighted coefficient; and Q is the total number of basis functions used.

It must be noted that the training sets should consist of a good number of reconstructions and the corresponding projections. It is required that the training sets should include the sample reconstructions that correspond to scenarios tht are as diverse as possible. Defining $\Psi = [\vec{\psi}_1, \vec{\psi}_2, \cdots, \vec{\psi}_K]$, and $\Phi = [\vec{\varphi}_1, \vec{\varphi}_2, \cdots, \vec{\varphi}_Q]$, it can be noted that these two matrices are unitary, and their inverse are the same as their transpose. Therefore, Eq. (2) can be rewritten as

$$M\vec{\alpha} = \vec{\beta}, \tag{6}$$

where $M = \Phi^T W \Psi$, $\vec{\alpha} = [\alpha_1, \alpha_2, \cdots, \alpha_K]^T$, $\vec{\beta} = [\beta_1, \beta_2, \cdots, \beta_Q]^T$. Typically, Eq. (6) is a small-scale linear equation system which can be solved efficiently in a least square sense [23] as

$$\vec{\alpha} = M^{\dagger}\vec{\beta}, \tag{7}$$

where $M^{\dagger}$ is the Moore–Penrose generalized inverse of M.

The setup used for the proof-of-concept experiment is illustrated in Fig. 2. As can be seen, two customized fiber bundles (Nanjing Chunhui Science and Technology Industrial Co., Ltd.), each with four input ends and one output end were used to collect the flame projections from eight perspectives.

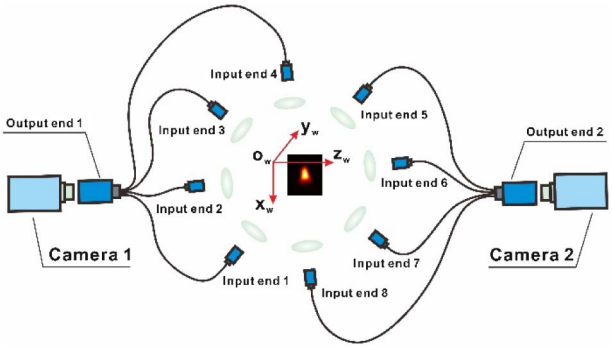

Fig. 2. Schematic of the endoscopic CTC system. Eight fiber bundles were used to collect the projections from different perspectives.

The input ends of the fiber bundles were arranged in nearly an equiangular manner so as to maximize the differences between the projections. The projections were then captured simultaneously by two synchronized cameras (Photron FASTCAM Mini AX100) which were operated at an exposure time of one millisecond and a frame rate of 1000 fps. The dimensions of the eight input ends and the two output ends are 8 mm × 8 mm and 16 mm × 16 mm, respectively. Each input end contains an array of ∼22, 000 multi-mode fibers. An AF Nikon lens (50 mm focal length and f/1.8) was positioned in front of each input end to collect the particular projection. The cameras are equipped with an AIS Nikon Micro lens (55 mm focal length and f/2.8) to relay the projections onto the complementary metal oxide semiconductor chips.

An arbitrary sequence of 60 consecutive frames and the following 60 frames were then selected for the training and testing purposes, respectively. Figure 3 shows an example set of eight projections of a Bunsen flame. The tomographic volume was set to be 6 mm × 6 mm × 6 mm in dimension and discretized into 60 × 60 × 60 voxels. The number of effective pixels i.e., the ones that covered the projections of the reconstruction volume, were estimated to be ∼80, 000. Thus, this inverse problem is highly underdetermined.

Due to the good performance of ART when a limited number of projections are available [24], it was adopted for the tomographic reconstructions of the 60 training samples. A detailed implementation of ART and parameter tuning can be found in [5]. Before the reconstructions, the images without the presence of the flame were taken and subtracted from the projections so as to remove the background. A multiplicative factor was then applied to the projections to ensure that their integrated intensity is consistent [25].

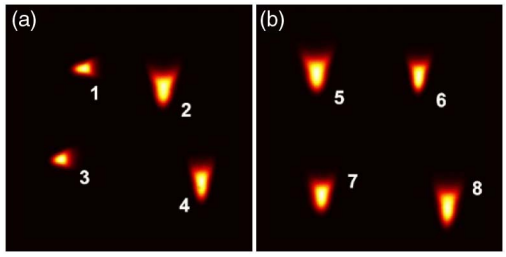

Fig. 3. Example set of eight projections of a Bunsen flame taken by the endoscopic CTC system.

The basis functions for both the reconstructions and projections can then be extracted from the training sets by performing the TPOD procedure. The number of basis functions used for reconstructions depend on how accurate the approximation is required to be. According to [26], the mean square error in the estimation directly correlates with the accumulated magnitude of the eigenvalues that correspond to the used eigenvectors. Thus, the selection criterion is suggested to be

$$\sum_{i=1}^{T} \lambda_i / \sum_{i=1}^{D} \lambda_i \geq \xi, \tag{8}$$

where λ_i is the ith eigenvalue; the parameters T and D are the used and total number of the basis functions, respectively; and ξ is the parameter that controls the mean square error of the estimation [26] and is set to 95% in this Letter.

Figure 4 plots the 60 eigenvalues for the training set of reconstructions, and the truncation parameter K was determined to be 5. Similarly, the parameter Q was determined to be 8. The selected basis functions were then used to calculate the matrix $M^{\dagger}$ and the vector β for each case in the testing set. By comparing Eqs. (2) and (6), we can see that the dimension of the inversion problem is reduced by ∼36, 000×.

The reconstructions for the testing set can then be obtained by solving Eq. (7). Panels 5(a) and 5(c) of Fig. 5 are the slices cut from the reconstructed 3D Bunsen flame for two randomly selected consecutive cases. The red cube and yellow parallelogram in each figure represent the reconstruction volume and

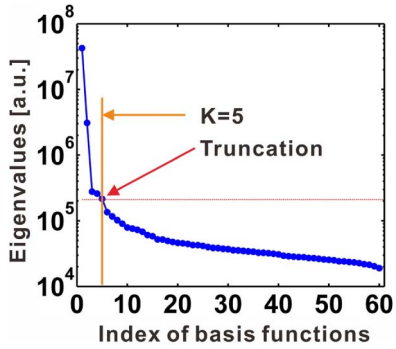

Fig. 4. 60 eigenvalues for the training set of reconstructions.

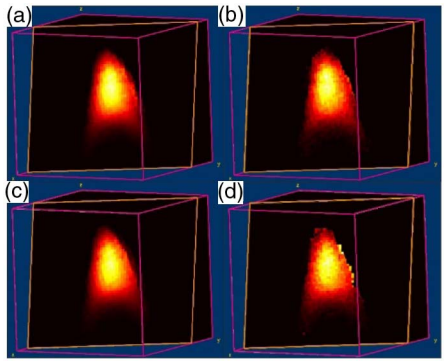

Fig. 5. Panels (a) and (c) are the slices cut from the reconstructed 3D Bunsen flame for two randomly selected consecutive cases using the TPOD method. Panels (b) and (d) are the counterparts obtained for the ART algorithm.

the cut slice, respectively. It is worth noting that the cut slice is not parallel with any of the three axes in the world coordinate system. The reconstructions from ART are also plotted in panels 5(b) and 5(d) for comparison. It can be seen that the reconstructions from both methods were in good agreement and conform to the practical Bunsen flame structure. Furthermore, the flame height was estimated to be 3.5 mm and was consistent with the value calculated from the size of the flame on the images and the magnification of the imaging system.

To further validate the effectiveness of the proposed method, the correlation coefficients between the reconstructions obtained from the TPOD method and the ART algorithm were calculated as

$$r = \frac{\sum_{i=1}^{I}(x_i - \bar{x})(y_i - \bar{y})}{\sqrt{\sum_{i=1}^{I}(x_i - \bar{x})^2} \cdot \sqrt{\sum_{i=1}^{I}(y_i - \bar{y})^2}}, \tag{9}$$

where x_i and y_i represent the ith element of reconstructions; and $\bar{x}$ and $\bar{y}$ are their mean values. The correlation coefficients for all the testing cases were plotted as a red line with solid circles in Fig. 6. The correlation coefficients between the simulated projections according to Eq. (5) using the TPOD reconstructions and the measured projections were also plotted as a blue line with solid squares in the figure. As can be seen, all these correlation coefficients were larger than 0.9, indicating the reconstructions calculated via the TPOD method were consistent with that obtained from the ART algorithm. This conclusion also agrees with our observations from Fig. 5.

On the other hand, the processing time for a tomographic reconstruction using the TPOD method was about 10 ms, which was much less then that 1155 s using the ART algorithm. All the cases were run at a desktop Intel(R) Xeon(R) 2.60 GHz CPU. The computational time can be further reduced by using a better CPU or employing parallel computing.

In summary, this Letter introduces a new tomographic reconstruction algorithm based on dimension reduction via POD for volumetric tomography as applied to combustion diagnostics. This method approximates the reconstruction as a weighted summation of a few representative KL-basis functions which are extracted from a training set. Such treatment greatly reduces the number of variables to be determined compared with the previous approach. The results obtained from the proof-of-concept experiment suggest that the reconstructions obtained are consistent with that from the ART algorithm.

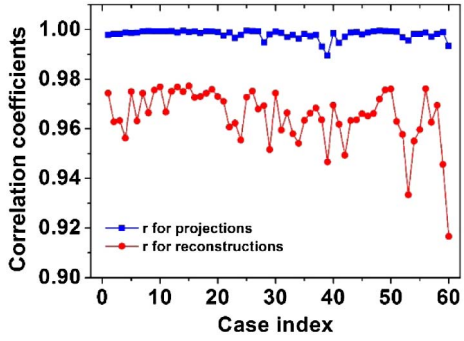

Fig. 6. Correlation coefficients between the reconstructions from TPOD and ART for 60 testing cases, and between the simulated projections according to Eq. (5) using the TPOD reconstructions and the measured projections.

However, the computational time the former required was ~100, 000× less than the latter one. Such capacity makes real-time 3D tomographic reconstruction more practical. Although this Letter is discussed under the context of endoscopic CTC, the TPOD method is expected to be also valuable to other tomographic modalities such as tomographic absorption spectroscopy [8,9,27,28], x-ray computed tomography [29], and electrical impedance tomography [30].

Funding. National Natural Science Foundation of China (NSFC) (51706141); Chinese Government "Thousand Youth Talent Program."

REFERENCES

1. M. Lin, Q. Lei, W. Yue, W. Xu, T. M. Ombrello, and C. D. Carter, Combust. Flame **165**, 1 (2016).
2. B. R. Halls, P. S. Hsu, N. Jiang, E. S. Legge, J. J. Felver, M. N. Slipchenko, S. Roy, T. R. Meyer, and J. R. Gord, Optica **4**, 897 (2017).
3. B. R. Halls, N. Jiang, T. R. Meyer, S. Roy, M. N. Slipchenko, and J. R. Gord, Opt. Lett. **42**, 2830 (2017).
4. T. R. Meyer, B. R. Halls, N. Jiang, M. N. Slipchenko, S. Roy, and J. R. Gord, Opt. Express **24**, 29547 (2016).
5. T. Yu, H. Liu, W. Cai, T. Yu, H. Liu, W. Cai, T. Yu, H. Liu, and W. Cai, Opt. Express **25**, 24093 (2017).
6. J. Floyd, P. Geipel, and A. M. Kempf, Combust. Flame **158**, 376 (2011).
7. J. Floyd and A. M. Kempf, Proc. Combust. Inst. **33**, 751 (2011).
8. T. Yu and W. Cai, Appl. Opt. **56**, 2183 (2017).
9. T. Yu, B. Tian, and W. Cai, Opt. Express **25**, 5982 (2017).
10. H. Liu, T. Yu, M. Zhang, and W. Cai, Appl. Opt. **56**, 7107 (2017).
11. W. Cai, X. Li, F. Li, and L. Ma, Opt. Express **21**, 7050 (2013).
12. J. Wang, Y. Song, Z. Li, A. Kempf, and A. He, Opt. Lett. **40**, 1231 (2015).
13. L. Ma, Q. Lei, J. Ikeda, W. Xu, Y. Wu, and C. D. Carter, Proc. Combust. Inst. **36**, 4575 (2016).
14. L. Ma, Y. Wu, Q. Lei, W. Xu, and C. D. Carter, Combust. Flame **166**, 66 (2016).
15. L. Ma, Y. Wu, W. Xu, S. D. Hammack, T. Lee, and C. D. Carter, Appl. Opt. **55**, 5310 (2016).
16. W. Cai and L. Ma, Appl. Opt. **49**, 601 (2010).
17. E. D. Torniainen and F. C. Gouldin, Combust. Sci. Technol. **131**, 85 (1998).
18. M. W. Kang, Y. Wu, and L. Ma, Combust. Flame **161**, 3063 (2014).
19. L. Ma, Q. Lei, Y. Wu, T. M. Ombrello, and C. D. Carter, Appl. Phys. B **119**, 313 (2015).
20. L. Sirovich and R. Everson, *Management and Analysis of Large Scientific Datasets* (Sage Publications, 1992), pp. 50–68.
21. B. D. Geraedts, S. Yang, C. M. Arndt, and A. M. Steinberg, in *AIAA Aerospace Sciences Meeting* (2015).
22. J. P. Moeck, J. F. Bourgouin, D. Durox, T. Schuller, and S. Candel, Exp. Fluids **54**, 1 (2013).
23. K. S. Banerjee, *Generalized Inverse of Matrices and Its Applications* (Wiley, 1971), p. 598.
24. N. A. Worth and J. R. Dawson, Meas. Sci. Technol. **24**, 24013 (2013).
25. B. R. Halls, D. J. Thul, D. Michaelis, S. Roy, T. R. Meyer, and J. R. Gord, Opt. Express **24**, 10040 (2016).
26. D. Kim, J. G. Lee, B. D. Quay, D. A. Santavicca, K. Kim, and S. Srinivasan, *ASME Turbo Expo 2008: Power for Land, Sea, and Air* (2008), pp. 757–765.
27. W. Cai and C. F. Kaminski, Prog. Energy Combust. Sci. **59**, 1 (2017).
28. J. Dai, S. O'Hagan, H. Liu, W. Cai, and P. Ewart, Appl. Phys. Lett. **111**, 184102 (2017).
29. A. M. G. Gentemann, C. Hirsch, K. Kunze, F. Kiesewetter, T. Sattelmayer, and W. Polifke, *International Gas Turbine and Aeroengine Congress & Exposition* (2004), pp. 501–510.
30. B. D. Bellows, M. K. Bobba, J. M. Seitzman, and T. Lieuwen, J. Eng. Gas Turbines Power **129**, 823 (2006).